Characterization of Heme-Regulated eIF2α Kinase: Roles of the N-Terminal Domain in the Oligomeric State, Heme Binding, Catalysis, and Inhibition†

Marketa Miksanova, Jotaro Igarashi, Masahiro Minami, Ikuko Sagami,‡ Seigo Yamauchi, Hirofumi Kurokawa, and Toru Shimizu*

Institute of Multidisciplinary Research for Advanced Materials, Tohoku University, Sendai 980-8577, Japan

Received March 21, 2006; Revised Manuscript Received May 22, 2006

ABSTRACT: Heme-regulated eIF2α kinase [heme-regulated inhibitor (HRI)] plays a critical role in the regulation of protein synthesis by heme iron. The kinase active site is located in the C-terminal domain, whereas the N-terminal domain is suggested to regulate catalysis in response to heme binding. Here, we found that the rate of dissociation for Fe(III)−protoporphyrin IX was much higher for full-length HRI (1.5×10^{-3} s^{-1}) than for myoglobin (8.4×10^{-7} s^{-1}) or the α-subunit of hemoglobin (7.1×10^{-6} s^{-1}), demonstrating the heme-sensing character of HRI. Because the role of the N-terminal domain in the structure and catalysis of HRI has not been clear, we generated N-terminal truncated mutants of HRI and examined their oligomeric state, heme binding, axial ligands, substrate interactions, and inhibition by heme derivatives. Multiangle light scattering indicated that the full-length enzyme is a hexamer, whereas truncated mutants (truncations of residues 1−127 and 1−145) are mainly trimers. In addition, we found that one molecule of heme is bound to the full-length and truncated mutant proteins. Optical absorption and electron spin resonance spectra suggested that Cys and water/OH^- are the heme axial ligands in the N-terminal domain-truncated mutant complex. We also found that HRI has a moderate affinity for heme, allowing it to sense the heme concentration in the cell. Study of the kinetics showed that the HRI kinase reaction follows classical Michaelis−Menten kinetics with respect to ATP but sigmoidal kinetics and positive cooperativity between subunits with respect to the protein substrate (eIF2α). Removal of the N-terminal domain decreased this cooperativity between subunits and affected the other kinetic parameters including inhibition by Fe(III)−protoporphyrin IX, Fe(II)−protoporphyrin IX, and protoporphyrin IX. Finally, we found that HRI is inhibited by bilirubin at physiological/pathological levels ($IC_{50} = 20$ μM). The roles of the N-terminal domain and the binding of heme in the structural and functional properties of HRI are discussed.

In eukaryotes, protein synthesis is terminated when cells face an emergency such as a shortage of amino acids, stress to the endoplasmic reticulum, and viral infection. Translation initiation is regulated by eukaryotic initiation factor 2α (α-subunit of eukaryotic initiation factor 2; eIF2α)[1] kinases (*1*−*3*). Four eIF2α kinases are known, including GCN2, PKR, PERK, and heme-regulated inhibitor (HRI) (*4*). These four eIF2α kinases phosphorylate Ser51 of eIF2α. Phosphorylated eIF2α binds tightly to eIF2B, a guanosine nucleotide exchange factor, resulting in the termination of protein synthesis (*3*). The kinase functions of GCN2, PERK, PKR, and HRI initiate the termination of protein synthesis when cells face emergencies, including amino acid starvation, stress to the endoplasmic reticulum, viral infection, and a shortage of heme iron, respectively (*5*−*8*). Although these four kinases have similar kinase domains, their sensing functions and domains differ (*5*−*8*).

HRI senses and mediates responses to changes in the heme concentration. Under normal conditions when there is sufficient heme, HRI does not phosphorylate eIF2α (*1*), but when there is a shortage of heme, it acts to maintain the heme-to-globin ratio at 1:1 by phosphorylating eIF2α, which initiates the termination of protein synthesis (*1*−*3*, *9*). Although HRI is reported to sense the heme concentration in reticulocytes or red blood cells (*9*), it is found in almost all tissues, including the brain (hippocampus, hypothalamus, and cerebellum), lung, heart, liver, spleen, kidney, thymus, stomach, pancreas, colon, testis, and uterus (*10*−*12*). Therefore, it appears that HRI functions not only in reticulocytes and red blood cells but also in these other tissues; however, the molecular mechanisms, in particular, the role of the N-terminal domain in its oligomerization, kinase function, and heme sensing, have remained elusive. In addition, little is known regarding how heme binds to the catalytic domain and regulates catalysis, the stoichiometry of heme binding, and which residues are axial ligands for the heme iron.

† This work was in part supported by Grants-in-Aid from the Ministry of Education, Culture, Sports, Science, and Technology of Japan to M.M. and T.S. This work was also supported in part by a Postdoctoral Fellowship for Foreign Researchers to M.M. from the Japan Society for the Promotion of Science (JSPS).

* To whom correspondence should be addressed. Tel: +81-22-217-5604, 5605. Fax: +81-22-217-5604, 5390. E-mail: shimizu@tagen.tohoku.ac.jp.

‡ Present address: Graduate School of Agriculture, Kyoto Prefectural University, Shimogamo, Sakyo-ku, Kyoto 606-8522, Japan.

[1] Abbreviations: HRI, heme-regulated eIF2α kinase or heme-regulated inhibitor; MALS, multiangle light scattering; eIF2α, α-subunit of eukaryotic initiation factor 2; SDS−PAGE, sodium dodecyl sulfate−polyacrylamide gel electrophoresis; Fe(III)−hemin, Fe(III)−protoporphyrin IX complex; Fe(II)−heme, Fe(II)−protoporphyrin IX complex; EPR, electron paramagnetic resonance; IRP2, iron regulatory protein 2; GCN2, general control nonderepressible 2; PKR, pancreatic eIF2α kinase; PERK, PKR-like ER kinase.

10.1021/bi060556k CCC: $33.50
Published on Web 07/25/2006

In the present study, to elucidate the role of the N-terminal domain in the structure and catalysis of HRI, we generated N-terminal truncated mutants and used multiangle light scattering (MALS) to examine the states of oligomerization of these mutants and the full-length enzyme. We also examined Fe(III)−protoporphyrin IX complex [Fe(III)−hemin] and Fe(II)−protoporphyrin IX complex [Fe(II)−heme] binding characteristics, electron paramagnetic resonance (EPR) spectra of the Fe(III)−hemin complex, and the catalytic functions under various conditions. We found marked differences in the state of oligomerization, hemin-binding characteristics, and heme axial ligands between the full-length and mutant proteins, whereas the kinetic functions and inhibition by hemin were not substantially different. Finally, we discuss the role of the N-terminal domain in the structure and function of HRI.

EXPERIMENTAL PROCEDURES

Materials. Restriction and modification enzymes were acquired from Takara Bio (Otsu, Japan), Toyobo (Osaka, Japan), New England Biolabs (Beverly, MA), and Nippon Roche (Tokyo, Japan). Other chemicals were purchased from Wako Pure Chemicals (Osaka, Japan).

Plasmid Construction. A plasmid encoding $(His)_6$-tagged wild-type HRI comprising residues 1−619 (His_6 HRI) from a mouse liver cDNA was originally constructed in the pET28 vector (Novagen, Madison, WI) as previously described (*13*). Because HRI has several thrombin cleavage sites (HRI sequence, LVVRNS; thrombin site, LVPRGS), we could not use thrombin to remove the $(His)_6$ tag. We thus introduced a PreScission protease (Amersham Biosciences, Piscataway, NJ) recognition site into the expression vector so that we could remove the $(His)_6$ tag. As a result, this protein has extra Gly-Pro-His residues prior to the Met residue. N-Terminal truncated mutants Δ85 (amino acids 86−619), Δ127 (amino acids 128−619), and Δ145 (amino acids 146−619) were prepared by PCR using the appropriate primers. The 5′-sense primers, which contained *Eco*RI and *Nde*I sites, were 5′-GGAATTCCATATGAAACAGGTGTTTAAATTAC-3′ for Δ85, 5′-GGAATTCCATATGAGGTCTGCCAAAGAGAG-3′ for Δ127, and 5′-GGAATTCCATATGCAGAAAATCAGATCCAG-3′ for Δ145; the 3′-antisense primer, which contained a stop codon and an *Eco*RI site, was 5′-CGAATTCTCATCTCTTCAGCCCTC-3′. The PCR products were first subcloned into the *Eco*RI site of the pBSKII(+) vector so that the sequences could be confirmed. The desired products were then digested with *Nde*I and *Eco*RI and then subcloned into the pET28a vector containing the PreScission protease recognition site to construct expression plasmids. A site-directed mutant, Lys196Arg, was constructed with a QuikChange mutagenesis kit (Stratagene, La Jolla, CA) using the following primers: 5′-sense (5′-TGGTCAGCATTATGCAATTAGGAAAATCCTGATTAAGAGCG-3′) and 3′-antisense (5′-CGCTCTTAATCAGGATTTTCCTAATTGCATAATGCTGACCA-3′). The plasmid encoding $(His)_6$-tagged eIF2α was constructed as previously described (*13*).

Protein Expression and Purification. $(His)_6$-tagged HRI was expressed in *Escherichia coli* BL21(DE3) Codon Plus RIL (Stratagene) harboring pET28a-PreScission/HRI (*13*) and then purified as described previously (*12*, *13*, *15*) with some modifications. Briefly, cell lysates containing apo-$(His)_6$-tagged HRI were isolated by 25−40% ammonium sulfate precipitation, and the isolated protein was then subjected to sequential chromatographic steps on DEAE-cellulose (DE52; Whatman, Maidstone, U.K.) and Ni^{2+}−NTA−agarose (Qiagen, Valencia, CA). Next, the $(His)_6$ tag was digested by PreScission protease and purified by Sephadex G-25 (HiTrap), GS-Trap, and His-Trap column chromatography (Amersham Biosciences) using the AKTA system (Amersham Biosciences). Purified $(His)_6$-tag-free HRI proteins were more than 95% homogeneous as determined by sodium dodecyl sulfate−polyacrylamide gel electrophoresis (SDS−PAGE; 7.5% gel) followed by staining with Coomassie Brilliant Blue R250. Protein concentrations were determined using the Coomassie Brilliant Blue dye binding method for protein (Nacalai Tesque, Kyoto, Japan). Final yields were 0.21, 0.34, 0.86, and 0.51 mg/L of culture for the full-length, Δ85, Δ127, and Δ145 mutants, respectively. $(His)_6$-tagged eIF2α was expressed and purified as previously described (*16*).

All proteins obtained in the present study were soluble and autophosphorylated, as confirmed by SDS−PAGE. Lys196 is reported to be essential for kinase activity and therefore autophosphorylation (*14*, *15*). When we mutated this residue to arginine to prevent autophosphorylation, the protein was retained in inclusion bodies and was difficult to solubilize, which is consistent with the idea that autophosphorylation is required for solubility.

Classical Size Exclusion Column Chromatography and Size Exclusion Column Chromatography with MALS Detection. We used size exclusion chromatography on Superdex 200HR 10/30 (Amersham Biosciences) to evaluate the oligomeric state of the purified proteins (71 μM full-length HRI, 66 μM Δ85 HRI, 83 μM Δ127 HRI, or 56 μM Δ145 HRI). The mobile phase was the buffer used for the in vitro kinase activity (20 mM Tris-HCl, pH 7.7, 150 mM KCl, and 2 mM magnesium acetate) supplemented with 1 mM dithiothreitol. The column was calibrated with the following molecular size standards: ribonuclease A (13.7 kDa), chymotrypsinogen A (25 kDa), ovalbumin (43 kDa), albumin (67 kDa), aldolase (158 kDa), catalase (232 kDa), ferritin (450 kDa), and thyroglobulin (669 kDa). A 100 μL sample of protein solution was applied to the column. The results indicated that all proteins used in the present study were soluble and not aggregated.

For MALS detection experiments, chromatography was carried out with the same mobile phase but using Shodex KW-804 and KW-802.5 columns (Showa Denko, Tokyo). A minDAWN tristar from Wyatt Technology Corp. (Santa Barbara, CA) was used as the detector for MALS. Aliquots (20 μL) of protein samples (71 μM full-length HRI, 66 μM Δ85 HRI, 83 μM Δ127 HRI, and 56 μM Δ145 HRI) were applied to two size exclusion columns that were connected in tandem (Shodex KW-804 and KW-802.5). The eluate was directly analyzed by using a multiangle light photometer (minDAWN tristar from Wyatt Technology Corp.). Light scattering response is directly proportional to the molecular mass of a sample. Therefore, the MALS method can measure the absolute molar mass of the eluting protein without column calibration or reference standards.

Optical Absorption Spectra. Optical absorption spectra were collected using a Shimadzu UV-2500 spectrophotom-

eter and a Shimadzu Multi Spec 1500 spectrophotometer (Kyoto, Japan) maintained at 25 °C. The optical absorption spectral changes were recorded under both aerobic and anaerobic conditions in 50 mM Tris-HCl, pH 8.0, buffer at 25 °C. The reaction mixture was incubated for 10 min prior to spectroscopic measurements to ensure that the temperature of the solution was stable and that the Fe(III)−hemin or Fe(II)−heme properly coordinates with the protein. Experiments were performed at least three times for each complex.

EPR Spectra. The Fe(III)−Δ145 mutant (80 μM) complex was prepared in 50 mM Tris-HCl, pH 8.0, containing 50% glycerol at 25 °C. EPR spectra were recorded on a JEOL FE-3X spectrometer (Tokyo, Japan) at 25 K. The magnetic field was calibrated using an NMR gauss meter (Echo Electronics, Hadsund, Denmark; model EFM-2000), and the temperature was controlled with an Oxford 900 cryosystem (*13*).

Stopped-Flow Measurements. Stopped-flow absorbance measurements for determining heme association rate constants were conducted using an RSP-1000 stopped-flow apparatus (Unisoku, Osaka, Japan) maintained at 25 °C (*31*). Association of CO−heme (0.25 μM) with different concentrations of full-length HRI (0.5−1.0 μM) was monitored at 423 nm (*19*). The reaction was initiated by mixing with excess apoprotein. Data were fitted using Igor-Pro (Wavemetrics, Inc., Lake Oswego, OR) (*19*, *20*). Experiments were conducted at least three times, and experimental errors were within 20%.

Heme Dissociation Experiments. All heme dissociation experiments were carried out in 1 cm path length, 1 mL volume cuvettes containing 800 μL of reaction mixture at 15−37 °C. For most experiments, this mixture consisted of 0.15 M potassium phosphate (pH 7.0), 0.45 M sucrose, 30 μM apomyoglobin (sperm whale) His64Tyr/Val68Phe mutant, and 3.0 μM stock HRI holoprotein solution. The pH values of these reaction mixtures never deviated more than 0.02 unit from that of the original solution. The reactions were initiated by adding holoprotein to the buffer−apomyoglobin mixture. Spectral changes were monitored at 410 nm as described previously (*20*). Experiments were conducted at least three times, and experimental errors were within 20%.

In Vitro Protein Kinase Assay. The in vitro protein kinase assay was conducted as described previously (*17*, *18*, *23*) with some modifications. Briefly, the kinase reaction mixture (20 μL) containing 20 mM Tris-HCl, pH 7.7, 2 mM magnesium acetate, 60 mM KCl, 2 μg of $(His)_6$-tagged eIF2α, 0.35 μM tag-free HRI (full-length and truncated mutant proteins), and 50 μM ATP was incubated at 15 °C for 10 min under aerobic conditions. The reaction was stopped by adding Laemmli sample buffer (62.5 mM Tris-HCl, pH 6.8, 10% glycerol, 2% 2-mercaptoethanol, 2% sodium dodecyl sulfate, and 0.002% bromophenol blue) and then heated for 10 min at 95 °C and subjected to 10% SDS−PAGE. Proteins were transferred onto poly(vinylidene difluoride) membranes (Bio-Rad, Hercules, CA). Phosphorylated proteins were detected by immunoblotting with an anti-phosphorylated eIF2α antibody (*13*) (Santa Cruz Biotechnology, Inc., Santa Cruz, CA).

Primary mouse anti-$(His)_6$ monoclonal IgM (H-3), goat anti-HRI IgG (S-16), rabbit anti-eIF2α IgG (FL-315), and goat anti-phosphorylated eIF2α IgG (Ser52) antibodies were purchased from Santa Cruz Biotechnology, Inc. For immunoblotting, the membrane was blocked for 1 h with 5% bovine serum albumin in Tris-buffered saline containing 0.1% Tween 20 (TBST) and incubated overnight at room temperature with primary antibody diluted in TBST. After being washed with TBST, the membrane was incubated with horseradish peroxidase-conjugated sheep anti-mouse IgG, donkey anti-rabbit IgG (Amersham Biosciences), or donkey anti-goat IgG (Santa Cruz Biotechnology) for 1 h. Immunoreactive protein bands were visualized using ECL reagents (Amersham Biosciences) and detected using a Fuji Film chemiluminescence reader, LAS-3000 IDX6 (Tokyo, Japan). The intensities of bands were calculated using Image J 1.32j (National Institutes of Health, Bethesda, MD) software. We compared the relative intensity of the corresponding bands (*13*).

Kinetic Analysis of eIF2α Phosphorylation. The assay mixture (20 μL) for the kinetic analysis of HRI contained 20 mM Tris-HCl, pH 7.7, 2 mM magnesium acetate, 60 mM KCl, 0.35 μM tag-free HRI full-length or N-terminal domain truncated mutant proteins, 0.5−4 μg of $(His)_6$-tagged eIF2α, and 2.5−100 μM ATP. The assay solution was incubated at 15 °C for 1 min (initial velocity conditions). The amount of reaction product (phosphorylated eIF2α) formed per minute during the first 2 min (determined by immunoblotting; see In Vitro Protein Kinase Assay) was equivalent to the initial velocity of the kinase reaction. Because the HRI kinase reaction is a bisubstrate reaction (ATP and eIF2α), the apparent kinetics for each substrate were determined in the presence of an excess of the other substrate. Kinetic constants were determined by nonlinear least-squares regression analysis using the Michaelis−Menten equation or the Hill equation as appropriate (*18*). Experiments were performed at least three times for each reaction mixture, and experimental errors were within 20%.

RESULTS

Oligomerization State. Although the molecular mass of HRI predicted from the amino acid sequence is 72 kDa, previous reports have estimated that it is between 180 and 640 kDa (*2*, *15*, *17*, *21*−*24*). The consensus is that HRI likely forms an elongated homodimer in aqueous solution (*15*). We used the MALS technique (*25*) in combination with size exclusion chromatography to precisely determine the state of HRI oligomerization. This method separated each protein as a distinct single band (Figure 1). Direct measurements by MALS detection indicated that the molecular masses in aqueous solution of full-length, Δ85, Δ127, and Δ145 N-terminal truncated mutants were 396, 371, 167, and 230 kDa, respectively (Table 1). In contrast, the molecular masses predicted from their amino acid sequences are 72, 63, 58, and 56 kDa, respectively. Therefore, it appears that the full-length and the Δ85 mutant proteins are hexamers, whereas the Δ127 and Δ145 proteins are mainly trimers. It should be pointed out that the proteins are soluble due to autophosphorylation (*14*, *15*).

Heme-Binding Characteristics. To determine the heme-binding characteristics of HRI, we monitored the absorption changes of Fe(III)−hemin upon addition of full-length wild-type and Δ145 mutant enzymes. As shown in Figure 2A, the Soret band at 422 nm increased upon addition of the full-length protein, although it increased less for the Δ145

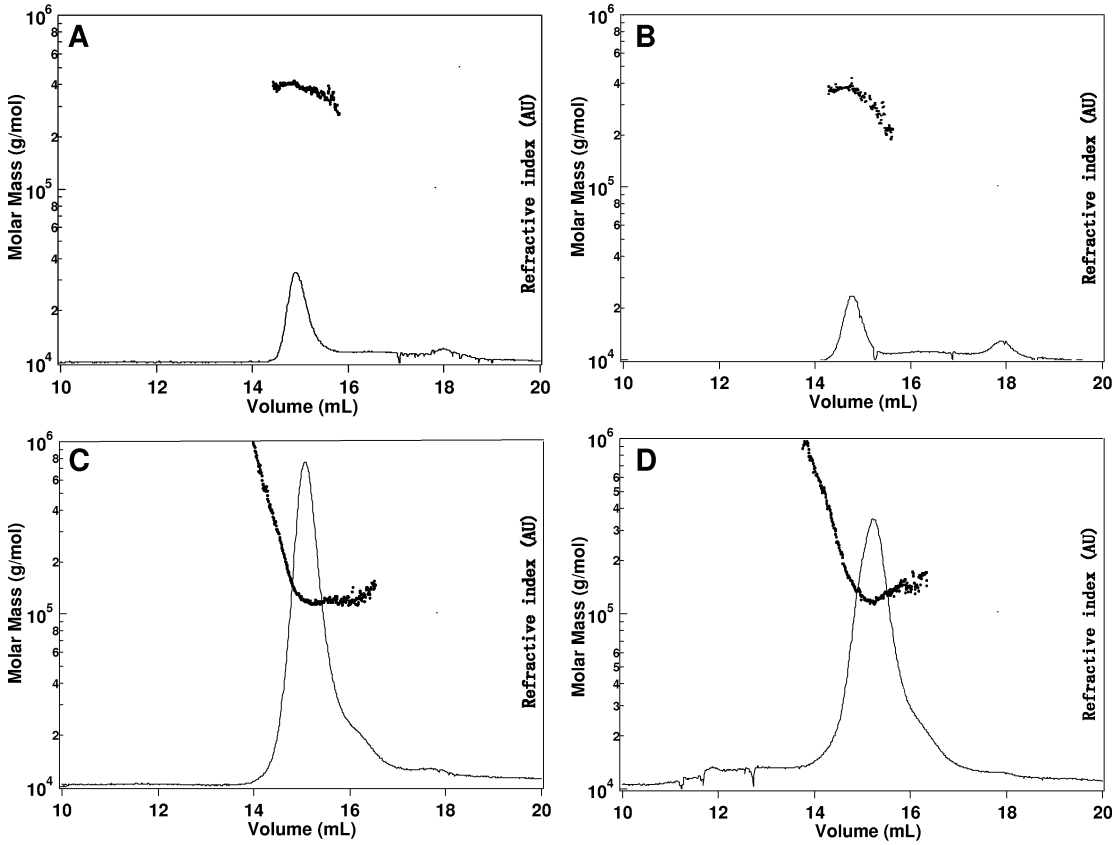

FIGURE 1: Determination of the absolute molecular mass of the full-length (A) and N-terminal truncated mutant proteins, Δ85 HRI (B), Δ127 HRI (C), and Δ145 HRI (D) by MALS. The molecular mass (dots) was calculated from MALS data and overlaid on the refractive index chromatogram (solid lines). Light scattering response (the peak of the solid line) directly corresponds with the molecular mass (dots) of the sample.

Table 1: Molecular Masses (kDa) of Full-Length Wild-Type and N-Terminal Truncated Mutants As Estimated from Amino Acid Sequences and As Determined by MALS[a]

HRI	full length	Δ85	Δ127	Δ145
theoretical (monomer)	72	63	58	56
SDS−PAGE	93.4	75.8	72.9	70.2
size exclusion[b]	447	446	342	326
MALS	396	371	167	230
MALS/theoretical	5.5	5.9	2.9	4.1
oligomerization	hexamer	hexamer	trimer	trimer

[a] The state of oligomerization was determined from the ratio of the mass determined by MALS to the theoretical mass based on the amino acid sequence. [b] The mobile phase was the reaction buffer used for the in vitro kinase assay (20 mM Tris, pH 7.7, 150 mM KCl, and 2 mM magnesium acetate supplemented with 1 mM dithiothreitol), and the solid phase was Superdex 200 HR 10/30. Protein concentrations used were approximately 4.5 mg/mL.

mutant than for the full-length protein (Figure 2B). We further conducted Fe(III)−hemin titration of full-length and Δ145 mutant enzymes. As shown in Figure 2C,D, the peak at 422 nm increased for the full-length protein, whereas, for the Δ145 mutant protein, there was an increase in the peak at 370 nm as well as the relatively small increase in the 422 nm band. Plots of the spectral increase at 370 nm for the Δ145 mutant protein versus the Fe(III)−hemin/protein ratio revealed a clear binding pattern for the 1:1 Fe(III)−hemin to protein complex (closed circles on solid lines in Figure 2F). Similarly, the plot of the 422 nm absorption for the full-length protein demonstrated that the stoichiometry of Fe(III)−hemin to protein was 1:1 (closed circles on solid lines in Figure 2E). Therefore, it appeared that a new species with an absorption at 370 nm was generated by adding Fe(III)−hemin to the Δ145 mutant protein. The same peak around 370 nm was observed in spectra of heme complexes of iron regulatory protein 2 (IRP2), another heme sensor protein (*39*), suggesting that the band around 370 nm is not due to a nonspecific binding of the Fe(III)−hemin to the Δ145 protein. Also, note that the spectrum of the free Fe(III)−hemin complex (the dashed line in Figure 2A,B) has broad peaks at approximately 387 and 357 nm, corroborating that the 370 nm species is not the free Fe(III)−hemin complex.

Addition of the Fe(II)−heme complex to the full-length and Δ145 mutant proteins under anaerobic conditions caused specific spectral changes (Figure 3A,B). For both proteins, the first phases of the titration plots for spectral changes at 426 or 425 nm saturated at certain points (Figure 3C,D), suggesting that, in both cases, one molecule of Fe(II)−heme binds specifically to one molecule of protein. Only the Δ145 mutant exhibited the characteristic absorbance at 390 nm. The band around 390 nm observed in the titration of the Δ145 protein is due to a coordinated complex rather than a nonspecific interaction because it could not be removed by size exclusion chromatography and, moreover, the free Fe(II)−heme complex has a broad Soret absorption at 409.5 nm. A similar absorption peak around 390 nm was observed in the spectra of heme complexes for another heme sensor protein, IRP2 (*39*). These results indicate that both full-length and Δ145 HRI can bind either Fe(III)−hemin or Fe(II)−heme in a 1:1 stoichiometry. The second phases are due to nonspecific binding.

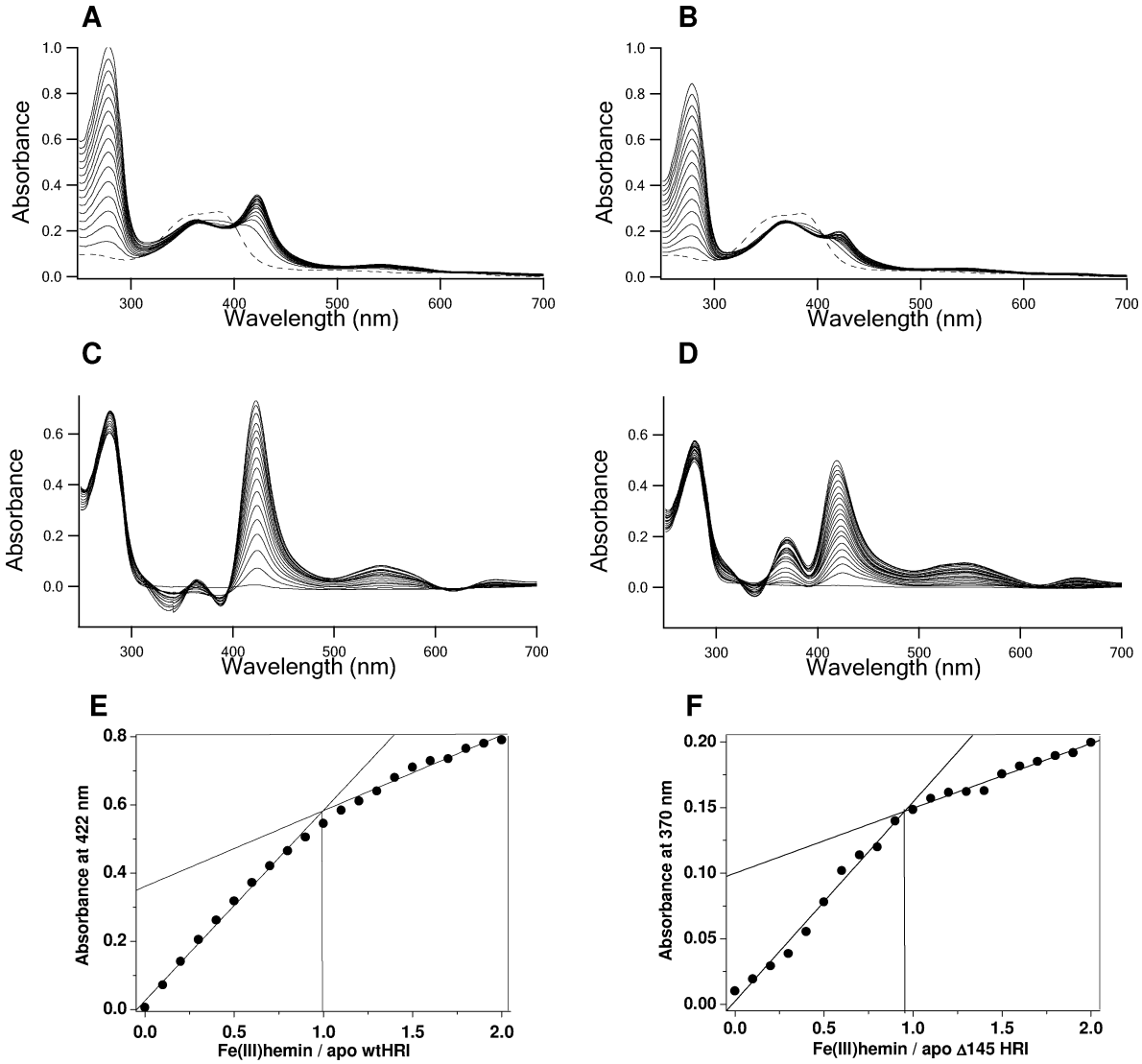

FIGURE 2: Optical absorption spectral changes of Fe(III)−hemin (5 μM) [free Fe(III)−hemin, dashed line] upon addition of the full-length (A) and the Δ145 mutant (B) proteins (1 μM each). Difference absorption spectral changes of Fe(III)−hemin for the full-length enzyme (10 μM) (C) and the Δ145 mutant (10 μM) (D) were obtained at the same concentrations of Fe(III)−hemin (1 μM each) as for references. According to the Soret spectral titration plots (closed circles) at 422 (E) and 370 nm (F) for full-length and Δ145 mutant proteins, respectively, both proteins form 1:1 Fe(III)−hemin to protein complexes. The absorption peak at 370 nm is not due to free Fe(III)−hemin, which has broad Soret peaks around 384 and 364 nm [dashed line in (A)].

EPR Spectra. To further characterize the axial ligands for the ferric heme in HRI, we performed EPR measurements (Figure 4). The full-length wild-type protein has an EPR spectrum typical of a cysteine thiolate and a histidine nitrogenous-coordinated (Cys/His) low-spin complex (*13*). The EPR spectrum (Figure 4A) of the Fe(III)−hemin complex of the Δ145 mutant protein contains both low- and high-spin heme signals as observed for cytochrome P450-type proteins (*47*, *48*, *53*). The Fe(III)−Δ145 HRI complex gave g values of low-spin ($g = 2.42$, 2.26, 1.91) and high-spin species ($g = 6.08$). Crystal field analysis of these low-spin signals gives tetragonality and rhombicity values similar to those of cytochrome P450 (*47*, *48*), suggesting that Cys and water/OH^- are the axial ligands in the Δ145 mutant (Table 2, Figure 4B). On the basis of EPR parameters, the axial ligands of the full-length HRI appear to be Cys and His (*13*). Because the Δ145 mutant lacks the N-terminal domain, it is reasonable to speculate that the His axial ligand should be located in the N-terminal domain, whereas the Cys axial ligand of the full-length HRI enzyme should be located in the C-terminal region. Removal of the N-terminal domain in the Δ145 mutant protein should have kept the original Cys ligand in the C-terminal domain but removed the original His trans to Cys, forcing it to take on water/OH^- as the new axial ligand.

Heme-Binding Kinetics. To investigate the role of the heme sensor in HRI function, we studied the association and dissociation kinetics and their temperature dependence for full-length HRI (Figure 5). As described above, the full-length HRI binds Fe(II)−heme and Fe(III)−hemin with a 1:1 stoichiometry. As shown in Figure 5A, the heme association kinetics fit well to a single-exponential equation, whereas the heme dissociation kinetics fit to a two-exponential equation (Figure 5C). We used the fast phase rate constant for characterizing heme dissociation, whereas the slower rate appeared to represent protein denaturation over the course of a long incubation. As summarized in Table 3, the association rate constant (k_{on}) of the heme from HRI was 1.1×10^7 M^{-1} s^{-1}, which is similar to the values obtained for other heme-binding proteins (*19*); however, the

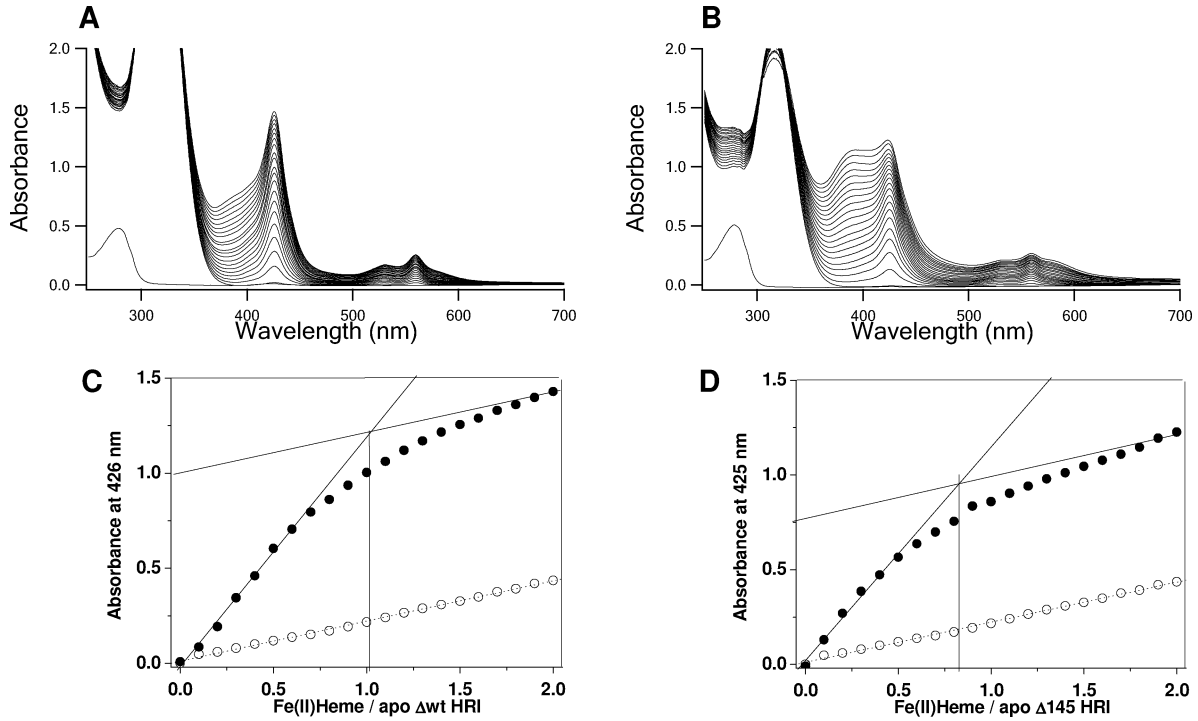

FIGURE 3: Optical absorption spectral change of the full-length (10 μM) (A) and Δ145 mutant (10 μM) (B) proteins caused by addition of Fe(II)−heme (1 μM each) under anaerobic conditions. Soret spectral titrations monitored at 426 and 425 nm for the full-length (C) and Δ145 mutant (D) proteins, respectively, indicate that both proteins form 1:1 Fe(II)−heme to protein complexes. In (C) and (D), the filled circles represent the actual spectral changes monitored at 426 and 425 nm for the full-length and Δ145 mutant proteins, respectively, whereas the open circles represent the increase in absorbance of the free Fe(II)−heme.

dissociation rate constant (k_{off}) for HRI (1.5×10^{-3} s^{-1}) was much higher than those of myoglobin (8.4×10^{-7} s^{-1}) and the α-subunit of hemoglobin (7.1×10^{-6} s^{-1}) (*19*, *20*). Rather, the k_{off} value of HRI was close to those of the His93Gly mutant of myoglobin (1.2×10^{-2} s^{-1}), the β-subunit of hemoglobin (9.4×10^{-4} s^{-1}), and bovine serum albumin (1.1×10^{-2} s^{-1}) (*19*, *20*). The activation energy of HRI, determined from the temperature dependency of the dissociation rate constant (Figure 5D), was 10.8 kJ mol^{-1}, which is also lower than the values for myoglobin (40.5 kJ mol^{-1}) (*19*) and the α-subunit of hemoglobin (69.1 kJ mol^{-1}) (*20*, *27*). These results suggest that heme dissociates from HRI much easier than from myoglobin or hemoglobin. Therefore, it appears that HRI has an affinity that allows sensing of the heme concentration in the cell.

Kinase Activity. To address the role of the N-terminal domain in catalysis, we examined the kinase activities of the full-length wild-type and N-terminal truncated mutant enzymes of HRI. We did not observe marked differences in the kinase activities between the full-length and the N-terminal truncated mutant enzymes (Figure 6A), suggesting that the N-terminal domain does not play a critical role in the activity of HRI.

Kinetic Analysis of eIF2α Phosphorylation. We further analyzed the kinetics of eIF2α phosphorylation by the full-length wild-type and N-terminal truncated mutant enzymes to determine the role, if any, of the N-terminal domain in the catalytic process. Because the kinase reaction catalyzed by HRI involves two substrates (ATP and eIF2α), we measured the apparent kinetic parameters for each substrate (Table 4 and Figure 6B,C). Interestingly, the phosphorylation of eIF2α showed classical Michaelis−Menten kinetics with respect to the ATP concentration (Figure 6B), whereas the kinetics were sigmoidal with respect to the concentration of eIF2α (Figure 6C), suggesting positive cooperation with eIF2α. This mechanism was observed for all enzymes studied, including the full-length wild-type and Δ145 mutant enzymes (Figure 6B,C). These results indicate that deletion of the N-terminal region does not significantly change the mechanism of the kinase reaction. Compared with the full-length enzyme, however, there was an increase in the maximal enzymatic velocities ($V_{max}^{eIF2\alpha}$ and V_{max}^{ATP} values) and the $K_{0.5}^{eIF2\alpha}$ for the Δ145 mutant (Table 4). Therefore, it appears that the N-terminal domain significantly suppresses catalysis although it also assists in the binding of eIF2α. Moreover, the Hill coefficient values decreased from approximately 3.8 for the full-length enzyme to 3.3 for the Δ145 mutant (Figure 6D). This also suggests that the N-terminal domain participates in the recognition of the substrate, eIF2α. Because the Hill coefficient describes the level of cooperation between subunits, the N-terminal domain increases the cooperativity of HRI with respect to eIF2α.

Inhibition by Heme and Porphyrin Derivatives. HRI works as a heme-based sensor enzyme wherein increasing the heme concentration inhibits catalysis. We examined the inhibition of the full-length wild-type and Δ145 mutant enzymes by Fe(III)−hemin. As seen in Figure 7, we did not observe a significant difference in the inhibition for the enzymes, although we did observe a 40% decrease in the IC_{50} value for the Δ145 mutant (Table 5). Interestingly, the Fe(III)−hemin inhibition curves for all tested enzymes were sigmoidal (S-shaped). Therefore, the kinase activity is not affected at low heme concentrations, but it is switched off at a certain high heme concentration (above the IC_{50}).

Cells may contain Fe(II)−heme, protoporphyrin IX, and heme metabolites such as bilirubin and biliverdin, as well

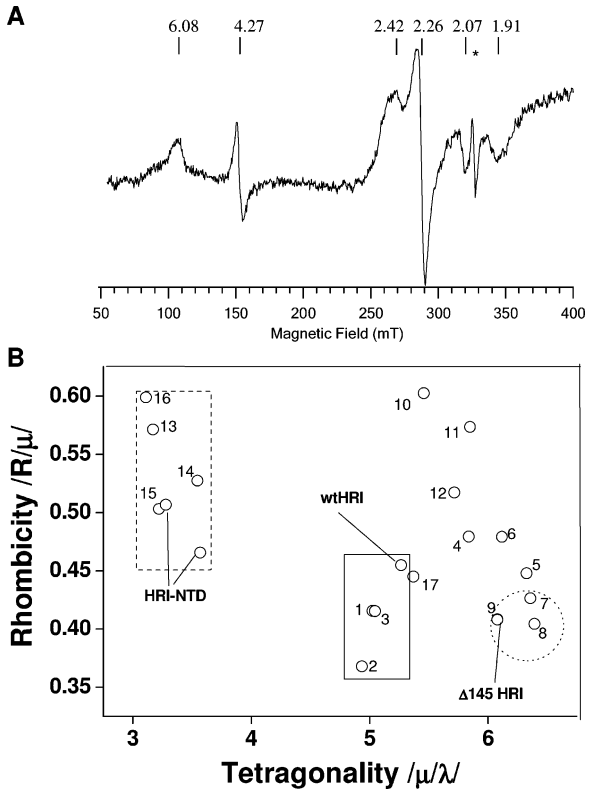

FIGURE 4: ESR spectra of the Fe(III)−Δ145 mutant HRI proteins (A) and crystal field analyses of *g* values for low-spin Fe(III) hemoproteins (B). (A) The ESR spectrum of the Fe(III)−Δ145 HRI complex (80 μM) in 50 mM Tris-HCl, pH 8.0 (at 25 °C), containing 50% glycerol was measured at 25 K. Spectra were accumulated 64 times. Conditions: modulation frequency and amplitude, 100 kHz and 1 mT, respectively; microwave frequency and power, 9.128069 GHz and 5 mW, respectively. (B) Crystal field diagram for low-spin Fe(III) hemoproteins. The numbers refer to the systems in Table 4. The areas surrounded by the solid (i), dashed (ii), and dotted lines (iii) contain His/Cys, His/His, and Cys/water or hydroxyl anion as the axial ligands, respectively.

as heme synthesis intermediates such as uroporphyrin, 5-aminolevulinic acid, and coproporphyrin. We therefore examined how these heme derivatives and other structurally related compounds influence HRI activity. As summarized in Table 5, the IC_{50} for Fe(II)−heme against the full-length enzyme was 2-fold lower than that for Fe(III)−hemin. Other heme metabolites only weakly inhibited HRI activity. Nevertheless, it is interesting that the IC_{50} values of the heme metabolites bilirubin and biliverdin were between 20 and 64 μM, which are within the levels found in pathological conditions (*28*, *29*). In contrast to the sigmoidal Fe(II)−heme and Fe(III)−hemin inhibition curves, the curves for all other tested HRI inhibitors were hyperbolic. The findings suggest that different sites of inhibition and/or mechanisms of inhibition are utilized by other degradation products and intermediates, emphasizing the importance of HRI as a heme sensor enzyme.

Site-Directed Mutagenesis. HRI phosphorylates itself at multiple sites and phosphorylates eIF2α at Ser51 (*3*, *14*, *18*, *30*). To understand the role of phosphorylation in the stability and activity of HRI, we mutated Lys196, which is essential for ATP binding and catalysis. The Lys196Arg mutant generated in the present study was very unstable and less soluble so that stable expression and purification of even a small amount of the protein was not feasible. This suggests that autophosphorylation of HRI is important for adequate solubility in the aqueous media and that the proteins used in the present study are soluble due to autophosphorylation.

Table 2: EPR *g* Values and Crystal Field Parameters for the Low-Spin Heme Complexes

	g values			crystal field parameters		
hemoprotein[a]	g_1	g_2	g_3	$\|\mu/\lambda\|$	$\|R/\mu\|$	ref
wild-type HRI	2.49	2.28	1.87	5.27	0.455	*13*
Δ145 HRI	2.42	2.26	1.91	6.08	0.408	this work
HRI-NTD	3.07	2.25	1.45	3.28	0.507	*13*
HRI-NTD	3.05	2.20	1.46	3.57	0.466	*40*
1. CBS, pH 8.5	2.5	2.3	1.86	5.03	0.416	*42*
2. CBS, pH 8.0, glycerol	2.51	2.33	1.87	4.93	0.368	*41*
3. CBS, pH 6.0	2.51	2.31	1.87	5.05	0.415	*41*
4. CooA	2.46	2.26	1.90	5.84	0.479	*43*−*45*
5. CooA, H77A	2.42	2.25	1.92	6.33		*43*
6. CooA, H77Y	2.44	2.25	1.91	6.12	0.479	*43*, *45*
7. P450	2.41	2.25	1.92	3.17	0.571	*47*
8. P450ARO	2.40	2.25	1.92	6.39	0.404	*47*
9. P450MIT	2.42	2.26	1.91	6.08	0.403	*48*
10. P450PB + *N*-MeIm	2.54	2.26	1.88	5.46	0.602	*47*
11. P450PB + *n*-oct amine	2.49	2.25	1.90	5.85	0.573	*47*
12. P450PB + Metyrapoe	2.48	2.26	1.89	5.72	0.517	*47*
13. HbA + imidazole	2.92	2.23	1.46	3.17	0.571	*49*
14. myoglobin, pH 9.6	2.93	2.22	1.52	3.55	0.527	*50*
15. cytochrome b_5, pH 6.2	3.05	2.22	1.41	3.22	0.503	*51*
16. LHb + imidazole	2.93	2.27	1.49	3.11	0.599	*52*
17. IRP2	2.47	2.27	1.87	5.37	0.445	*39*

[a] The numbers correspond with those in Figure 4B. Abbreviations: HRI-NTD, N-terminal domain of HRI; P450PB, rat liver microsomal cytochrome P450 induced by phenobarbital; P450ARO, rat liver microsomal cytochrome P450 induced by Aroclor 1254; P450MIT, cytochrome P450 in bovine adrenal cortex submitochondrial particles; *N*-MeIm, *N*-methylimidazole; *n*-oct amine, *n*-octylamine; LHb, leghemoglobin.

DISCUSSION

The N-Terminal Domain Is Critical for Maintaining the Oligomeric State. The molecular mass of the full-length HRI protein calculated by SDS−PAGE in the present study was 93.4 kDa (Table 1), which is higher than the value (72 kDa) estimated from its amino acid sequence. The increase may be partly due to added negative charges by multiple autophosphorylation. The phosphorylation is required for the HRI solubility (*3*, *14*, *18*, *30*). Similar increase in the molecular mass calculated by SDS−PAGE was observed for all N-terminal domain-truncated mutants (Table 1). Furthermore, chromatography patterns for each protein were single peaks, suggesting that they are homogeneous.

The state of HRI oligomerization has been a controversial issue. Several laboratories have reported that the molecular mass of HRI is 290 kDa (*17*, *21*, *22*, *24*) or 320 kDa (*2*), and one laboratory reported it as 180 kDa (*23*). A recent report indicated that HRI is in equilibrium between 420 and 640 kDa forms and that HRI exists as an elongated homodimer (*15*). In the current study, the molecular masses determined by classical size exclusion chromatography were 447, 446, 342, and 326 kDa for the full-length, Δ85, Δ127, and Δ145 mutant proteins, respectively. The molecular mass for the full-length enzyme is close to the recently reported value of 420 kDa (*15*). It is suggested that the MALS method can determine the exact molecular mass of oligomeric macromolecules such as polymers and proteins in aqueous

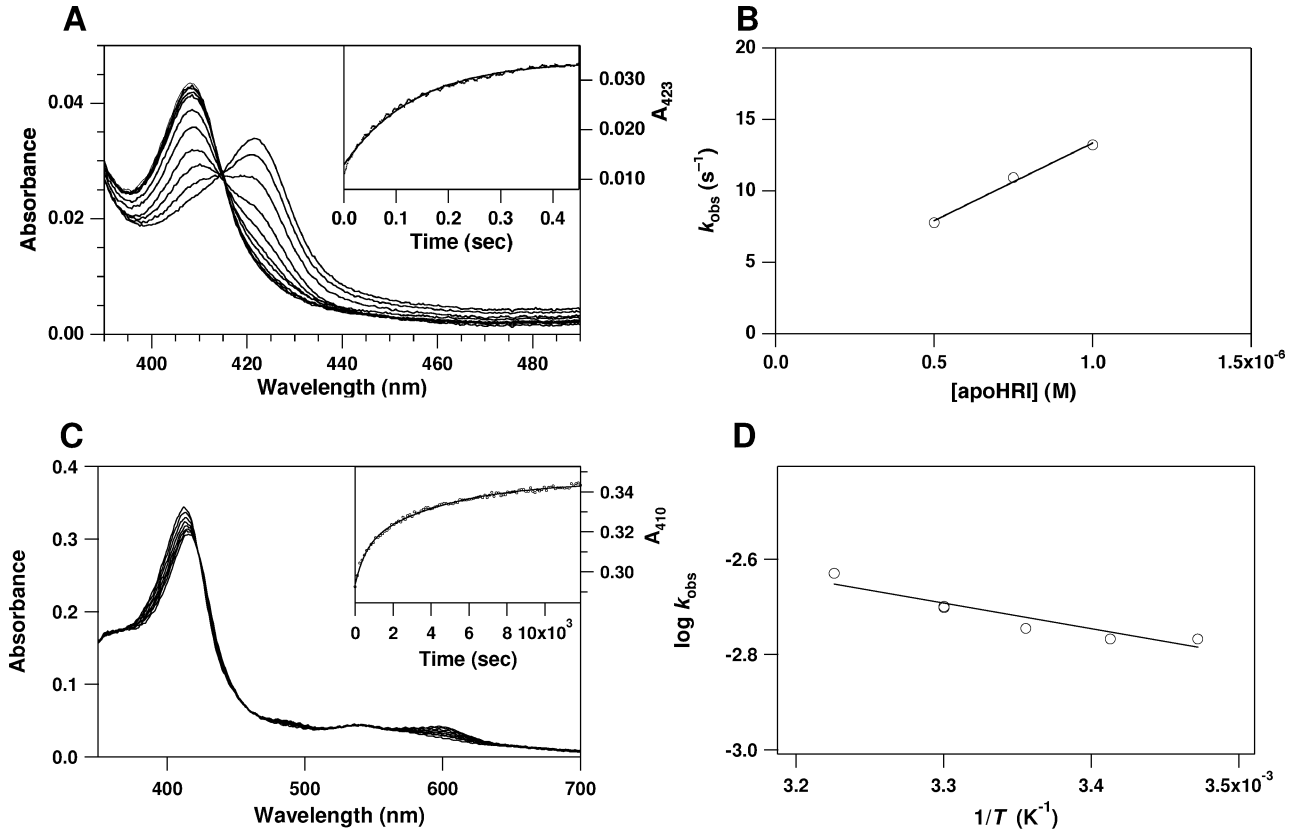

FIGURE 5: Heme-binding kinetics and temperature dependences. (A) Spectral changes accompanying the association of the CO−heme complex and the full-length enzyme. Association of CO−heme (0.25 μM) with different concentrations of full-length HRI (0.5−1.0 μM) was monitored at 423 nm. The inset shows the spectral changes at 423 nm. (B) The association rate was dependent on the concentration of full-length HRI. (C) Hemin dissociation from Fe(III)−HRI (3 μM) in the presence of excess apo H64Y/V68F sperm whale myoglobin (30 μM). The inset shows the spectral changes at 410 nm. (D) Arrhenius plot for the hemin dissociation rate constant vs the temperature.

Table 3: Heme Association and Dissociation Rate Constants for HRI and Other Heme-Binding Proteins[a]

	k_{on} ($M^{-1}\,s^{-1}$)	k_{off} (s^{-1})	K_d (M)	ΔE (kJ mol^{-1})	ref
HRI	1.1×10^7	1.5×10^{-3}	1.4×10^{-10}	10.8	this work
Mb	7.0×10^7	8.4×10^{-7}	1.2×10^{-14}	40.5	*19*, *27*
Mb H93G	7.0×10^7	1.2×10^{-2}	1.7×10^{-10}	nr	*19*
Hb	2.9×10^7	7.1×10^{-6} (α)	2.5×10^{-13}	69.1	*19*, *20*, *27*
		9.4×10^{-4} (*β*)	3.2×10^{-11}	49.0	*19*, *20*, *27*
BSA	5.0×10^7	1.1×10^{-2}	2.2×10^{-10}	nr	*19*

[a] Abbreviations: Mb, sperm whale myoglobin; Mb H93G, the His93Gly mutant of sperm whale myoglobin; Hb, hemoglobin, BSA, bovine serum albumin; nr, not reported. Note that k_{on} values were obtained for the Fe(II)−CO complex, whereas the k_{off} values were obtained for the Fe(III) complex.

media (*25*, *26*). The molecular masses evaluated by the MALS method were 396, 371, 167, and 230 kDa for the full-length, Δ85, Δ127, and Δ145 mutant enzymes, respectively. The molecular masses estimated from the amino acid sequences and MALS results suggest that the full-length and Δ85 mutant proteins exist as hexamers. Although the MALS results indicate that Δ127 and Δ145 mutant proteins are a mixture of trimers, tetramers, and larger oligomers, it appears that they were mostly trimers. This indicates that the N-terminal domain is critical for maintaining the hexameric state of the full-length HRI protein. These results agree with the kinetic analyses in that removal of the N-terminal domain decreases the cooperativity of HRI with respect to the eIF2α concentration.

One Molecule of Heme Binds to the Full-Length HRI, Probably with One Axial Ligand from the N-Terminal Domain and the Other from the Kinase Domain. Earlier reports suggested that there are two heme-binding sites in HRI, one in the N-terminal domain and the other in the kinase insert region, which lies between two kinase lobes (*37*); however, it has not been clear whether HRI binds one or two molecules of heme. The present study clearly showed that there is just a single molecule of heme bound to the full-length HRI. The ratio between full-length HRI and heme is 1:1 regardless of whether the titrations were performed using Fe(III)−hemin or Fe(II)−heme. Interestingly, we demonstrated that one molecule of heme is also bound by the Δ145 mutant (N-terminal domain-deleted mutant). Changes in the optical absorption spectra accompanied by heme binding indicated that heme binds specifically to the full-length enzyme. EPR and optical absorption spectral results revealed that heme is coordinated to full-length HRI by cysteine and histidine residues (*13*, *31*). On the other hand, in the present study, heme binding to the Δ145 mutant is different, resulting in a new species with a Soret peak around 370 and 390 nm for Fe(III)−hemin and Fe(II)−heme

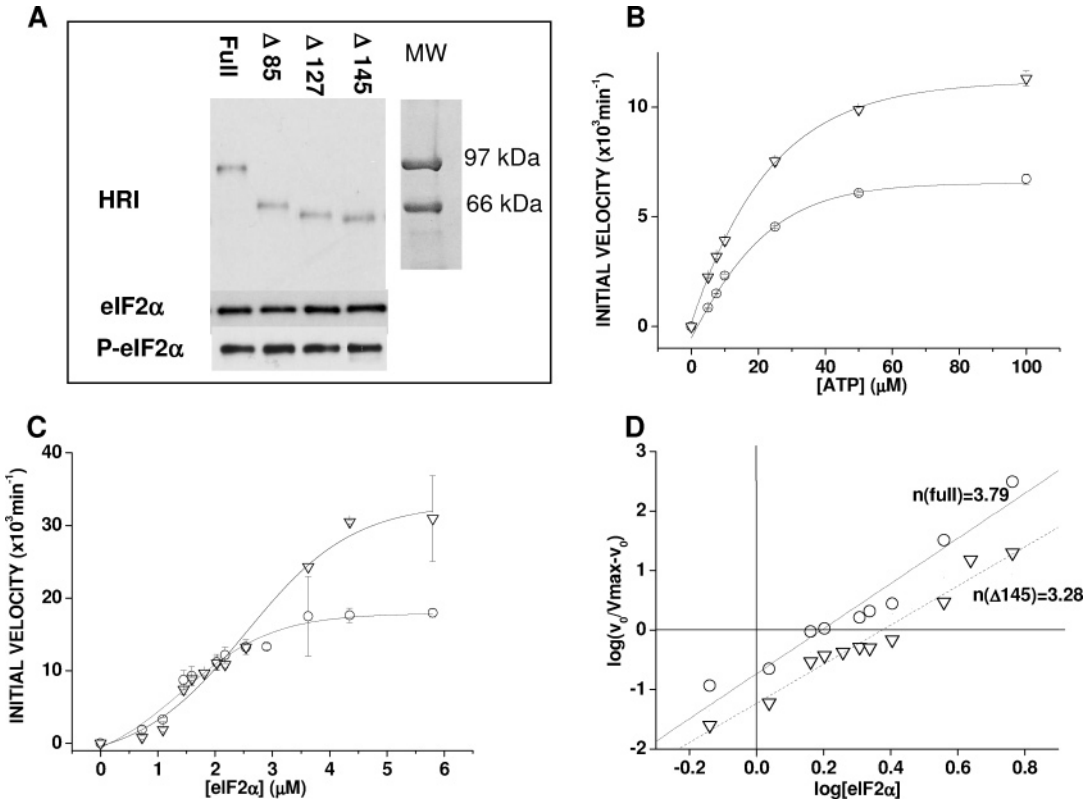

FIGURE 6: Kinetic analysis of eIF2α phosphorylation by full-length and the N-terminal domain-deleted HRI. (A) Evaluation of the kinase activities for the full-length and the N-terminal domain-deleted HRI proteins using eIF2α as a substrate. See details about the kinase assay in Experimental Procedures. After the samples were subjected to 10% SDS−PAGE proteins were transferred onto poly(vinylidene difluoride) membranes. The eIF2α and phosphorylated eIF2α proteins were detected by immunoblotting with anti-eIF2α (middle panel) and anti-phorphorylated eIF2α (bottom panel). The upper panel shows the total amount of full-length and the N-terminal domain-deleted mutant proteins as detected by staining the transfer membrane with 0.1% amido black. (B, C) Kinetic analysis of eIF2α phosphorylation by full-length (open circles) and Δ145 mutant (open triangle) enzymes. The kinetics are hyperbolic with respect to the ATP concentration (B) and sigmoidal with respect to the eIF2α concentration (C). (D) Hill plots of kinetics with respect to the eIF2α concentration for the heme-free full-length (open circle) and Δ145 mutant (open triangle) enzymes. Kinetic constants were determined by nonlinear least-squares regression analysis using the Hill equation (*18*).

Table 4: Apparent V_{max}, K_m, and $K_{0.5}$ Values and Hill Coefficients for ATP and eIF2α for the Full-Length and Δ145 Mutant Enzymes

	full length	Δ145
V_{max}^{ATP} (int units/min)	9600	16000
K_m^{ATP} (μM)	31	30
$V_{max}^{eIF2\alpha}$ (int units/min)	18000	33000
$K_{0.5}^{eIF2\alpha}$ (μM)[a]	1.7	2.6
$K_{0.5}^{eIF2\alpha}$ (μM)[b]	1.6	2.5
Hill coefficient	3.8	3.3

[a] $K_{0.5}$ values were obtained from the sigmoidal dose−response curve. [b] $K_{0.5}$ values were obtained from Hill plots.

binding, respectively. We suggest that cysteine in the C-terminal region, perhaps in the kinase domain, can serve as an alternative heme axial ligand because EPR spectral parameters of the Fe(III)−hemin complex of the Δ145 mutant are located in the region corresponding to Cys and water/OH^- as axial ligands (Scheme 1 and Figure 4B).

The kinase activity of the Δ145 mutant was clearly inhibited by the addition of heme even though the optical absorption spectrum showed different binding characteristics than the full-length HRI enzyme. It is possible that heme binds to the isolated kinase domain by a specific interaction, as demonstrated by the spectral change upon binding of heme by the Δ145 mutant. We suggest that the cysteine ligand responsible for the ligation of heme in the Δ145 mutant is identical to the cysteine ligand in the full-length HRI that acts in a trans configuration with respect to the His axial ligand of the N-terminal domain. Consequently, in the case of the Δ145 mutant, removal of the His axial ligand by deletion of the entire N-terminal domain results in emergence of the Cys coordination, and therefore, the new species observed in the absorption spectra and the EPR results.

Heme dissociation from the full-length HRI enzyme is fast compared with the dissociation of myoglobin and hemoglobin. In addition, the activation energy of heme binding to HRI is lower than that for myoglobin and hemoglobin. Therefore, it appears that the binding of heme to HRI is weaker than the binding of myoglobin and hemoglobin, which is reasonable because HRI is a heme-sensing enzyme.

The N-Terminal Domain Is Not Critical for Catalysis, but It Interacts with the Kinase Domain. Kinase activities for the full-length and the N-terminal truncated mutant enzymes were similar. This suggests that the N-terminal domain is not critical for catalysis by HRI. This has also been found for other heme-based sensor enzymes such as soluble guanylate cyclase (*33*) and *Ec* DOS (*34*), where the truncation of the heme-bound sensor domain does not significantly affect the catalytic activity.

For the Δ145 mutant, we observed a significant increase in $V_{max}^{eIF2\alpha}$ and in $K_{0.5}^{eIF2\alpha}$ compared to the full-length enzyme. The N-terminal domain, therefore, may interact with the catalytic site to some extent, covering the substrate

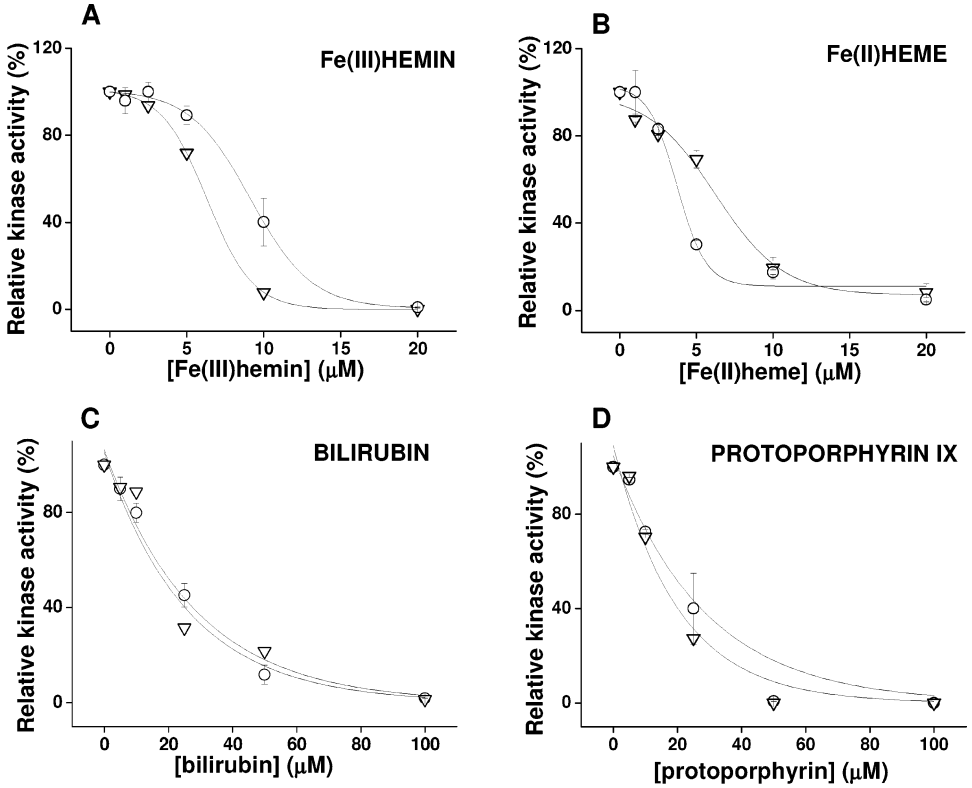

FIGURE 7: Inhibition of full-length (open circle) and Δ145 mutant (open triangle) enzymes by Fe(III)−hemin (A), Fe(II)−heme (B), bilirubin (C), and protoporphyrin IX (D). Inhibitors were dissolved in 0.5 μL of 0.1 M NaOH to yield final concentrations of 0.5−100 μM. An equal volume of 0.1 M NaOH alone was added to the control reaction mixture. See details about the kinase assay in Experimental Procedures.

Table 5: IC_{50} Values (μM) for Hemin and Other Derivatives

	full length	Δ145
Fe(III)−hemin	9.5	6.3
Fe(II)−heme	4.1	6.4
protoporphyrin IX	22.0	15.8
bilirubin	20.0	21.7
biliverdin	63.9	nd
uroporphyrin	81.8	nd
5-aminolevulinic acid	234	nd
coproporphyrin	>500	nd

Scheme 1: Proposed Structures of the Heme-Bound Wild-Type (Upper) and Δ145 Mutant (Lower) HRI Proteins Based on the Heme-Binding Characteristics and Heme Coordination Structures Determined in the Current Studies

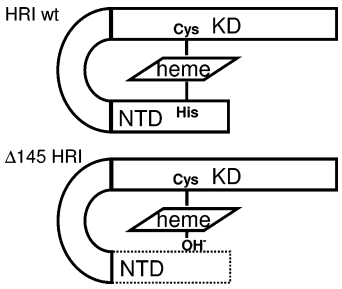

binding site, thereby reducing catalysis and substrate binding. Yun et al. (*38*) examined interactions between the N-terminal domain and the kinase domain and suggested that HRI's activity is regulated through modulation of the interaction between its N-terminal and catalytic domains.

Rafie-Kolpin et al. (*37*) reported that truncation of the N-terminal 103 and 130 amino acids of rabbit HRI decreases the specific activity from 5.64 min^{-1} for the full-length enzyme to 3.49 and 2.72 min^{-1}, respectively. Our results, however, indicate that the turnover number of the Δ145 mutant is similar to that of the full-length enzyme and that V_{max}^{ATP} is increased by truncation of the 144 N-terminal amino acids of mouse HRI.

Allosteric Effects. Interestingly, the full-length and the Δ145 mutant enzymes are allosterically regulated by the substrate, eIF2α, but not by the cosubstrate, ATP. As stated above, full-length HRI is hexameric, whereas the Δ145 mutant enzyme is trimeric. Thus, it is reasonable that interactions between the subunits influence the catalytic behavior associated with binding of the eIF2α protein but not the small molecule, ATP. X-ray crystallographic studies on the PKR−eIF2α complex (*54*) showed that PKR interacts with eIF2α via the former's C-lobe including Thr451, Thr487, and Glu490, residues that are conserved in all eIF2α kinases including HRI. Thus, the eIF2α protein may interact simultaneously with more than one subunit, producing the positive cooperativity. In addition, site-directed mutagenesis studies on PKR (*55*) showed that Thr487 is important for eIF2α recognition but PKR does not show any cooperativity with respect to the substrate concentration. Our results seem to indicate that the cooperativity is a unique characteristic of HRI.

Inhibition by Heme and Porphyrin Derivatives. The N-terminal domain-deleted mutant, Δ145, was more sensitive to Fe(III)−hemin inhibition (IC_{50} = 6.3 μM) than the full-length enzyme (IC_{50} = 9.5). Thus, when the N-terminal domain is truncated, it may be easier for Fe(III)−hemin to inhibit catalysis due to enhanced access to the active site.

Our results further demonstrated that the heme iron is important for the inhibition of HRI because protoporphyrin

IX is much less potent than Fe(III)−hemin and Fe(II)−heme. The Fe(II) cation has, in general, a higher affinity for nitrogen ligands than the Fe(III) cation. This accounts for the lower IC_{50} value (4.1 μM) of Fe(II)−heme than of Fe(III)−hemin (9.5 μM) for inhibition of the full-length enzyme, in which we suspect heme is coordinated by His and Cys. In contrast, heme binding to the isolated kinase domain (Δ145 mutant) appears to be cysteine-like in that it was equally sensitive to Fe(II)−heme and Fe(III)−hemin. Further studies must be conducted to address the mechanism of the heme binding to the Δ145 mutant.

The sigmoidal shape of the inhibition curves for Fe(III)−hemin and Fe(II)−heme is probably important for the heme-sensing properties of HRI. A sigmoidal curve means that the kinase activity is not affected at low heme concentrations but that higher concentrations cause a rapid and effective inhibition of the HRI kinase activity, allowing for the initiation of protein synthesis.

It is also interesting that heme metabolites such as biliverdin and bilirubin, which are products of heme oxygenase and biliverdin reductase, respectively, inhibit HRI. Under unusual conditions such as acute hepatitis, the concentration of the heme metabolite bilirubin increases up to 200 μM (*35*, *36*). Therefore, it is possible that accumulation of these heme metabolites in blood can endanger the subtle balance of protein synthesis. Thus, although a shortage of heme acts as a signal to activate the HRI kinase and thereby terminate protein synthesis, heme degradation products can also inhibit HRI, allowing protein synthesis to proceed. Because HRI is present not only in red blood cells but also in numerous tissues and organs (*10*−*12*), HRI may regulate protein synthesis in a variety of tissues in response to heme availability. It is reasonable to speculate, therefore, that HRI activity is inhibited and that protein synthesis is strongly influenced by the accumulation of the heme metabolites in acute disease. Moreover, heme metabolites, especially bilirubin, are known to be neurotoxic (*36*). We speculate that this could be due, at least in part, to an imbalance in protein synthesis caused by pathological concentrations of bilirubin.

SUMMARY

In summary, we evaluated the role of the N-terminal domain in structural and functional properties of HRI. We found that (i) the N-terminal domain is critical for maintaining the oligomeric state of HRI, (ii) the N-terminal domain interacts with the kinase domain but is not critical for the kinase activity, (iii) the N-terminal domain increases the cooperativity between subunits and probably assists in substrate recognition, (iv) only a single molecule of heme binds to the full-length HRI protein, and (v) the heme iron is coordinated with a histidine residue from the N-terminal domain and a cysteine residue of the kinase domain.

ACKNOWLEDGMENT

We thank Dr. John S. Olson (Rice University) for kindly providing the expression plasmid for His64Tyr/Val68Phe apomyoglobin. In addition, we thank Shingo Suzuki for assistance in constructing the deletion mutant plasmids. We also acknowledge Shoko Co., Ltd. (Tokyo, Japan), for allowing us access to their MALS detector and for valuable suggestions.

REFERENCES

1. Chen, J. J., and London, I. M. (1995) Regulation of protein synthesis by heme-regulated eIF-2α kinase, *Trends Biochem. Sci. 20*, 105−108.
2. Chefalo, P. J., Oh, J., Rafie-Kolpin, M., Kan, B., and Chen, J. J. (1998) Heme-regulated eIF-2α kinase purifies as a hemoprotein, *Eur. J. Biochem. 258*, 820−830.
3. Chen, J. J. (2000) in *Translational Control of Gene Expression* (Soneberg, N., Hershey, J. W. B., and Mathews, M. B., Eds.) pp 529−546, Cold Spring Harbor Laboratory, Cold Spring Harbor, NY.
4. Dever, T. E. (2002) Gene-specific regulation by general translation factors, *Cell 108*, 545−556.
5. Chen, J.-J., Throop, M. S., Gehrke, L., Kuo, I., Pal, J. K., Brodsky, M., and London, I. M. (1991) Cloning of the cDNA of the heme-regulated eukaryotic initiation factor 2α (eIF-2α) kinase of rabbit reticulocytes: homology to yeast GCN2 protein kinase and human doublestranded-RNA-dependent eIF-2α kinase, *Proc. Natl. Acad. Sci. U.S.A. 88*, 7729−7733.
6. Meurs, E., Chong, K., Galabru, J., Thomas, N. S., Kerr, I. M., Williams, B. R., and Hovanessian, A. G. (1990) Molecular cloning and characterization of human double-stranded RNA activated protein kinase induced by interferon, *Cell 62*, 379−390.
7. Chong, K. L., Feng, L., Schappert, K., Meurs, E., Donahue, T. F., Friesen, J. D., Hovanessian, A. G., and Williams, B. R. (1992) Human p68 kinase exhibits growth suppression in yeast and homology to the translational regulator GCN2, *EMBO J. 11*, 1553−1562.
8. Harding, H. P., Zhang, Y., and Ron, D. (1999) Protein translation and folding are coupled by an endoplasmic-reticulum-resident kinase, *Nature 397*, 271−274.
9. Crosby, J. S., Lee, K., London, I. M., and Chen, J.-J. (1994) Erythroid expression of the heme-regulated eIF-2α kinase, *Mol. Cell. Biol. 14*, 3906−3914.
10. Petrov, T., Rafols, J. A., Alousi, S. S., Kupsky, W. J., Johnson, R., Shah, J., Shah, A., and Watson, C. (2003) Cellular compartmentalization of phosphorylated eIF2α and neuronal NOS in human temporal lobe epilepsy with hippocampal sclerosis, *J. Neurol. Sci. 209*, 31−39.
11. Mellor, H., Flowers, K. M., Kimball, S. R., and Jefferson, L. S. (1994) Cloning and characterization of cDNA encoding rat hemin-sensitive initiation factor-2α (eIF-2α) kinase. Evidence for multitissue expression, *J. Biol. Chem. 269*, 10201−10204.
12. Berlanga, J. J., Herrero, S., and Haro, C. (1998) Characterization of the hemin-sensitive eukaryotic initiation factor 2α kinase from mouse nonerythroid cells, *J. Biol. Chem. 273*, 32340−32346.
13. Igarashi, J., Sato, A., Kitagawa, T., Yoshimura, T., Yamauchi, S., Sagami, I., and Shimizu, T. (2004) Activation of heme-regulated eukaryotic initiation factor 2α kinase by nitric oxide is induced by the formation of a five-coordinated NO-heme complex: Optical absorption, electron spin resonance, and resonance Raman spectral studies, *J. Biol. Chem. 279*, 15752−15762.
14. Rafie-Kolpin, M., Han, A. P., and Chen, J. J. (2003) Autophosphorylation of threonine 485 in the activation loop is essential for attaining eIF2α kinase activity of HRI, *Biochemistry 42*, 6536−6544.
15. Bauer, B. N., Rafie-Kolpin, M., Lu, L., Han, A., and Chen, J. J. (2001) Multiple autophosphorylation is essential for the formation of the active and stable homodimer of heme-regulated eIF2α kinase, *Biochemistry 40*, 11543−11551.
16. Zhu, S., Sobolev, A. Y., and Wek, R. C. (1996) Histidyl-tRNA synthetase-related sequences in GCN2 protein kinase regulate in vitro phosphorylation of eIF-2, *J. Biol. Chem. 271*, 24989−24994.
17. Chen, J. J., Yang, J. M., Petryshyn, R., Kosower, N., and London, I. M. (1989) Disulfide bond formation in the regulation of eIF-2α kinase by heme, *J. Biol. Chem. 264*, 9559−9564.
18. Mellor, H., and Proud, C. G. (1991) A synthetic peptide substrate for initiation factor-2 kinases, *Biochem. Biophys. Res. Commun. 178*, 430−437.
19. Hargrove, M. S., Barrick, D., and Olson, J. S. (1996) The association rate constant for heme binding to globin is independent of protein structure, *Biochemistry 35*, 11293−11299.

20. Hargrove, M. S., Singleton, E. W., Quillin, M. L., Ortiz, L. A., Phillips, G. N., Jr., Olson, J. S., and Mathews, A. J. (1994) His64(E7)→Tyr apomyoglobin as a reagent for measuring rates of hemin dissociation, *J. Biol. Chem. 269*, 4207−4214.
21. Gross, M., and Rabinovitz, M. (1972) Control of globin synthesis by heme: factors influencing formation of an inhibitor of globin chain initiation in reticulocyte lysates, *Biochim. Biophys. Acta 287*, 340−352.
22. Trachsel, H., Ranu, R. S., and London, I. M. (1978) Regulation of protein synthesis in rabbit reticulocyte lysates: purification and characterization of heme-reversible translational inhibitor, *Proc. Natl. Acad. Sci. U.S.A. 75*, 3654−3658.
23. Kudlicki, W., Fullilove, S., Read, R., Kramer, G., and Hardesty, B. (1987) Identification of spectrin-related peptides associated with the reticulocyte heme-controlled α subunit of eukaryotic translational initiation factor 2 kinase and of a Mr 95000 peptide that appears to be the catalytic subunit, *J. Biol. Chem. 262*, 9695−9701.
24. Yang, J. M., London, I. M., and Chen, J. J. (1992) Effects of hemin and porphyrin compounds on intersubunit disulfide formation of heme-regulated eIF-2α kinase and the regulation of protein synthesis in reticulocyte lysates, *J. Biol. Chem. 267*, 20519−20524.
25. Wittgren, B., Stefansson, M., and Porsch, B. (2005) Interactions between sodium dodecyl sulphate and non-ionic cellulose derivatives studied by size exclusion chromatography with online multi-angle light scattering and refractometric detection, *J. Chromatogr. A 1082*, 166−175.
26. Tarazona, M. P., and Saiz, E. (2003) Combination of SEC/MALS experimental procedures and theoretical analysis for studying the solution properties of macromolecules, *J. Biochem. Biophys. Methods 56*, 95−116.
27. Rose, M. Y., and Olson, J. S. (1983) The kinetic mechanism of heme binding to human apohemoglobin, *J. Biol. Chem. 258*, 4298−4303.
28. Van Hoydonck, P. G., Temme, E. H., and Schouten E. G. (2001) Serum bilirubin concentration in a Belgian population: the association with smoking tatus and type of cigarettes, *Int. J. Epidemiol. 30*, 1465−1472.
29. Manach, C., Williamson, G., Morand, C., Scalbert, A., and Remesy, C. (2005) Bioavailability and bioefficacy of polyphenols in humans. I. Review of 97 bioavailability studies, *Am. J. Clin. Nutr. 81*, 230S−242S.
30. Colthurst, D. R., Campbell, D. G., and Proud, C. G. (1987) Structure and regulation of eukaryotic initiation factor eIF-2: Sequence of the site in the alpha subunit phosphorylated by the haem-controlled repressor and by the double-stranded RNA-activated inhibitor, *Eur. J. Biochem. 166*, 357−363.
31. Igarashi, J., Sato, A., Kitagawa, T., Sagami, I., and Shimizu, T. (2003) CO binding study of mouse heme-regulated eIF-2α kinase: Kinetics and resonance Raman spectra, *Biochim. Biophys. Acta 1650*, 99−104.
32. Gilles-Gonzalez, M. A., and Gonzalez, G. (2005) Heme-based sensors: defining characteristics, recent developments, and regulatory hypotheses, *J. Inorg. Biochem. 99*, 1−22.
33. Martin, E., Sharina, I., Kots, A., and Murad, F. (2003) A constitutively activated mutant of human soluble guanylyl cyclase (sGC): Implication for the mechanism of sGC activation, *Proc. Natl. Acad. Sci. U.S.A. 100*, 9208−9213.
34. Yoshimura, T., Sagami, I., Sasakura, Y., and Shimizu T. (2003) Relationships between heme incorporation, tetramer formation, and catalysis of a heme-regulated phosphodiesterase from *Escherichia coli*: a study of deletion and site-directed mutants, *J. Biol. Chem. 278*, 53105−53111.
35. Dufour, D. R., Lott, J. A., Nolte, F. S., Gretch, D. R., Koff, R. S., and Seeff, L. B. (2000) Diagnosis and monitoring of hepatic injury. II. Recommendations for use of laboratory tests in screening, diagnosis, and monitoring, *Clin. Chem. 46*, 2050−2068.
36. Ostrow, J. D., Pascolo, L., Brites, D., and Tiribelli, C. (2004) Molecular basis of bilirubin-induced neurotoxicity, *Trends Mol. Med. 10*, 65−70.
37. Rafie-Kolpin, M., Chefalo, P. J., Hussain, Z., Hahn, J., Uma, S., Matts, R. L., and Chen, J. J. (2000) Two heme-binding domains of heme-regulated eukaryotic initiation factor-2α kinase. N terminus and kinase insertion, *J. Biol. Chem. 275*, 5171−5178.
38. Yun, B. G., Matts, J. A. B., and Matts, R. L. (2005) Interdomain interactions regulate the activation of the heme-regulated eIF2α kinase, *Biochim. Biophys. Acta 1725*, 174−181.
39. Ishikawa, H., Kato, M., Hori, H., Ishimori, K., Kirisako, T., Tokunaga, F., and Iwai, K. (2005) Involvement of heme regulatory motif in heme-mediated ubiquitination and degradation of IRP2, *Mol. Cell 19*, 171−181.
40. Ishikawa, H., Yun, B. G., Takahashi, S., Hori, H., Matts, R. L., Ishimori, K., and Morishima, I. (2002) NO-induced activation mechanism of the heme-regulated eIF2 kinase, *J. Am. Chem. Soc. 124*, 13696−13697.
41. Omura, T., Sadano, H., Hasegawa, T., Yoshida, Y., and Kominami, S. (1984) Hemoprotein H-450 identified as a form of cytochrome P-450 having an endogenous ligand at the 6th coordination position of the heme, *J. Biochem. (Tokyo) 96*, 1491−1500.
42. Ojha, S., Hwang, J. Kabil, O., Penner-Hahn, J. E., and Banerjee, R. (2000) Characterization of the heme in human cystathionine β-synthase by X-ray absorption and electron paramagnetic resonance spectroscopies, *Biochemistry 39*, 10542−10547.
43. Aono, S., Ohkubo, K., Matsuo, T., and Nakajima, H. (1998) Redox-controlled ligand exchange of the heme in the CO-sensing transcriptional activator CooA, *J. Biol. Chem. 273*, 25757−25764.
44. Reynolds, M. F., Shelver, D., Kerby, R. L., Parks, R. B., Roberts, G. P., and Burstyn, J. N. (1998) EPR and electronic absorption spectroscopies of the CO-sensing CooA protein reveal a cysteine-ligated low-spin ferric heme, *J. Am. Chem. Soc. 120*, 9080−9081.
45. Dhawan, I. K., Shelver, D., Thorsteinsson, M. V., Roberts, G. P., and Johnson, M. K. (1999) Probing the heme axial ligation in the CO-sensing CooA protein with magnetic circular dichroism spectroscopy, *Biochemistry 38*, 12805−12813.
46. Bohan, T. L. (1977) Analysis of low-spin ESR spectra of ferric heme proteins: a reexamination, *J. Magn. Reson. 26*, 109−118.
47. Ruf, H. H., Ahr, H., Nastainczyk, W., Ulrich, V., Mansuy, D., Battioni, J.-P., Montiel-Montoya, R., and Trautwein, A. (1984) Formation of a ferric carbanion complex from halothane and cytochrome P-450: electron spin resonance, electronic spectra, and model complexes, *Biochemistry 23*, 5300−5306.
48. Whysner, J. A., Ramseyer, J., and Harding, B. W. (1970) Substrate-induced changes in visible absorption and electron spin resonance properties of adrenal cortex mitochondrial P450, *J. Biol. Chem. 245*, 5441−5449.
49. Yonetani, T., Iizuka, T., and Waterman, M. R. (1971) Studies on modified hemoglobins. III. Spin states of ferric hemoglobin, semihemoglobin, and isolated subunit chains, *J. Biol. Chem. 246*, 7683−7689.
50. Gadsby, P. M., and Thomson, A. J. (1982) Identification of the imidazolate anion as a ligand in metmyoglobin by near-infrared magnetic circular dichroism spectroscopy, *FEBS Lett. 150*, 59−63.
51. Ikeda, M., Iizuka, T., Takao, H., and Hagihara, B. (1974) Studies of the heme environment of oxidized cytochrome b_5, *Biochim. Biophys. Acta 336*, 15−24.
52. Maskall, C. S., Gibson, J. F., and Dart, P. J. (1977) Electron-paramagnetic-resonance studies of leghaemoglobins from soya-bean and cowpea root nodules. Identification of nitrosyl-leghaemoglobin in crude leghaemoglobin preparations, *Biochem. J. 167*, 435−445.
53. Salerno, J. C., Frey, C., McMillan, K., Williams, R. F., Masters, B. S., and Griffith, O. W. (1995) Characterization by electron paramagnetic resonance of the interactions of L-arginine and L-thiocitrulline with the heme cofactor region of nitric oxide synthase, *J. Biol. Chem. 270*, 27423−27428.
54. Dar, A. C., Dever, T. E., and Sicheri, F. (2005) Higher-order substrate recognition of eIF2α by the RNA-dependent protein kinase PKR, *Cell 122*, 887−900.
55. Dey, M., Cao, C., Dar, A. C., Tamura, T., Ozato, K., Sicheri, F., and Dever, T. E. (2005) Mechanistic link between PKR dimerization, autophosphorylation, and eIF2α substrate recognition, *Cell 122*, 901−913.

BI060556K